

On the organization of grid and place cells: Neural de-noising via subspace learning

David M. Schwartz^{*1} and O. Ozan Koyluoglu^{†2}

¹Department of Electrical and Computer Engineering, University of Arizona

²University of California, Berkeley

Abstract

Place cells in the hippocampus are active when an animal visits a certain locations (referred to as place fields) within an environment and remain silent otherwise. Grid cells in the medial entorhinal cortex (MEC) respond at multiple locations, with firing fields that exhibit a hexagonally symmetric periodic pattern. The joint activity of grid and place cell populations, as a function of location, forms a neural code for space. An ensemble of codes, for a given set of parameters, is generated by selecting grid and place cell population and tuning curve parameters. For each ensemble, codewords are generated by stimulating a network with a discrete set of locations. In this manuscript, we develop an understanding of the relationships between coding theoretic properties of these combined populations and code construction parameters. These observations are revisited by measuring the performances of biologically realizable algorithms (e.g. neural bit-flipping) implemented by a network of place and grid cell populations, as well as interneurons, which perform de-noising operations. Simulations demonstrate that de-noising mechanisms analyzed here can significantly improve fidelity of this neural representation of space. Further, patterns observed in connectivity of each population of simulated cells suggest the existence of heretofore unobserved neurobiological phenomena.

1 Introduction

Place cells are spatially modulated neurons with bivariate Gaussian tuning curves centered on particular locations in the environment, and have been identified in the hippocampus [1]. Grid cells are spatially modulated neurons that exhibit a peak firing rate at a periodic and hexagonally symmetric distribution of locations in the environment, and are found in the Entorhinal Cortex (EC) of rats, mice, bats, and humans [2–4]. Grid cells are clustered in discrete modules wherein cells share grid scale. Anatomically, both cell types share a dorsoventral organization, with cells possessing wider receptive fields distributed towards the ventral end [5,6]. It is known that the rat grid cell network requires communication from the hippocampus to maintain grid-like activity [7],

^{*}dmschwar@email.arizona.edu

[†]ozan.koyluoglu@berkeley.edu

and that a significant improvement in accuracy of the rodent place cell representation is tightly correlated with the emergence of the grid cell network [8]. However, the mechanisms by which these networks communicate and how each may bolster the other’s accuracy are unknown.

Associative memories are a class of biologically implementable content addressable memory consisting of networks of neurons, a learning rule, and in some instances, a separate recall process [9]. This means that they can be exploited to stabilize the states of their constituent neurons to match a previously memorized network state if enough of the network already lies in this state. The information capacity of the simplest of these constructions is quite limited: $\frac{n}{2\log n}$ bits, for a network of n binary neurons [10]. However, recent advances by Salavati et al. take advantage of sparse neural coding and non-binary neurons to design an associative memory with information storage capacity exponential in the number of neurons [11]. Sparse connectivity confers the memory network with other performance improvements: infrequent spiking implies reduced energy costs and faster convergence to a stable state. In communications, this principle is leveraged by LDPC codes, whose power (in coding and decoding complexity) depends on sparsity of the code’s parity check matrix (an object analogous to our matrix of synaptic weights that form the de-noising network).

Grid cell population activity forms a dense modulo code, in which (in the absence of noise) information about position at any grid scale may be present in the activity of each module [2]. Biologically reasonable decoders for the grid cell position code were proposed and tested in [12], and we replicated these results by implementing the same grid cell population decoder, though it is not the focus of this paper. Place cell activity forms a relatively sparse code (for enough cells, and a sufficiently large environment), thus combining populations of grid and place cells realizes position codes that are sparser than the grid cell component of the code. Our results indicate that there are reasonable (in the biological sense) grid and place cell network parameters that result in population codes for position with a wide range of densities. Nature provides myriad circumstances in which many neural computations (e.g. object recognition, acoustic source localization, and self location) must be executed robustly in the presence of neural noise if the organism is to survive. We propose a de-noising mechanism for populations of grid and place cells, in the form of the associative memories described in [11], [13], and [14], which takes advantage of coding theoretic properties of these populations to eliminate the negative impacts of external noise. In particular, we propose a de-noising algorithm that relies on the biological organization of grid cells into discrete modules, and observe that after learning, average connectivity between place cells and grid modules decreases with increasing place cell size for each module.

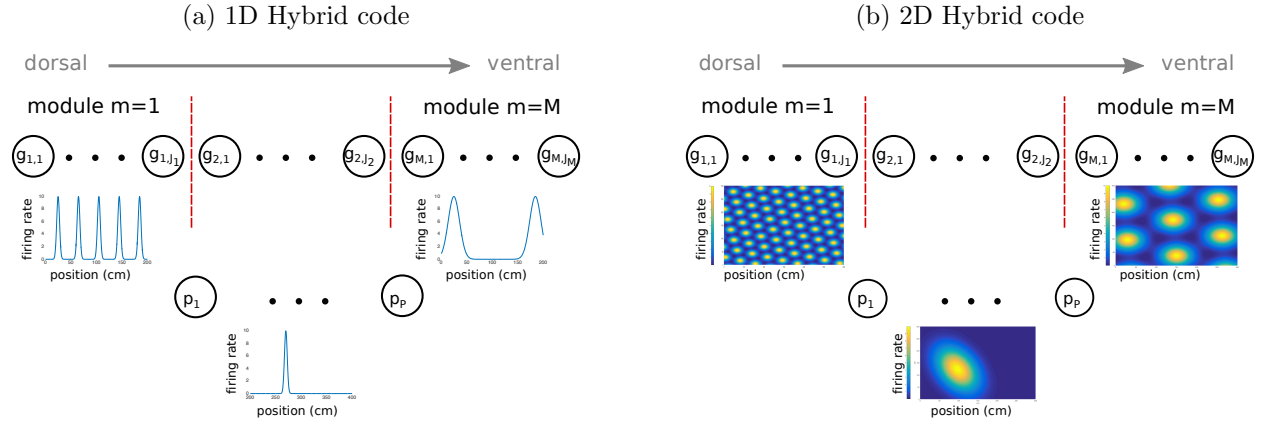
Redundancy in receptive field (RF) population codes is known to confer improvements in decoding accuracy when a small tolerance to error is introduced (expressed in this case, in the stimulus space to which we decode) [15]. We believe we are the first to investigate coding theoretic impacts of redundancy in grid cells. We investigate the impact of this redundancy on decoding accuracy by comparing de-noising and decoding performance across codes of varying redundancies. We demonstrate that a maximum likelihood (ML) estimator reliably decodes position from population activity with small position estimation error in the presence of bounded noise. Overall, our work shows that the biological organization of grid cells into modules may be necessary for optimal estimation

of self location.

This paper is organized sectionally. In section 1 we introduce a few key concepts and present the main results. Section 2 describes the theoretical framework upon which our model is built. Section 3 presents results of all coding theoretic analysis and experimentation. Section 4 describes the learning algorithms implemented in our de-noising network, as well as the outcomes of these learning algorithms. In section 5, we describe the de-noising processes and address their biological plausibility. Additionally, we present the results of performance tests of the ML position estimator, with and without de-noising. Section 6 consists primarily of discussion of these results.

2 Theoretical framework

2.1 A hybrid code



We consider a population of place and grid cells, a total of N neurons. There are M grid cell modules, each module, m , containing J_m neurons. Each grid cell is denoted as $\mathbf{G}_{m,j} \sim \text{Poisson}(g_{m,j})$, for $m \in \{1, \dots, M\}$ and $j \in \{1, \dots, J_m\}$. Place cells are denoted as $\mathbf{P}_i \sim \text{Poisson}(p_i)$, for $i \in \{1, \dots, P\}$. The activity of this population, as a function of the (1D) location ℓ , is represented by

$$\mathbf{x}_i(\ell) = \begin{cases} g_{m,j}(\ell), & i = \sum_{k=1}^{m-1} J_k + j, i \leq \sum_{m=1}^M J_m \\ p_{i-MJ}(\ell), & i > \sum_{m=1}^M J_m \end{cases}$$

where the location dependent mean firing rates of the grid cells, $g_{m,j}(\ell)$, are given by the following periodic Gaussian tuning curve

$$g_{m,j}(\ell) = f_{\max} \exp \left(\frac{-(\text{mod}(\lambda_m/2 + \ell - \phi_j, \lambda_m) - \lambda_m/2)^2}{2\sigma_m^2} \right). \quad (1)$$

Here, λ_m and σ_m are, respectively, the period and tuning widths of grid cells in module m , and ϕ_j is a random spatial phase. Each $p_i(\ell)$ is modeled as a thresholded Gaussian distribution over

$[0, L]$, where L is the length of a 1-dimensional track, with mean, μ , a random variable uniformly distributed over $[0, L]$, standard deviation, σ , chosen randomly and uniformly from $[0.9\lambda_1, 1.1\lambda_M]$.

We also consider a population of grid and place cells receptive to position in two dimensions. In this paradigm, each grid cell's tuning curve follows a two-dimensional distribution resembling a von-Mises density function,

$$g_{m,j}(\mathbf{s}) = \frac{f_{\max}}{Z} \exp \left[\sum_{k=1}^3 \cos \left(\frac{4}{\lambda_m \sqrt{3}} \mathbf{u}(\theta_k - \theta_{m,j}) \cdot (\mathbf{s} - \mathbf{c}_{m,j}) + \frac{3}{2} \right) - 1 \right], \quad (2)$$

where $\mathbf{u}(\theta_k - \theta_{m,j})$ is a unit vector in the direction of $\theta_k - \theta_{m,j}$, $\mathbf{s} \in [0, L] \times [0, L]$ is the position stimulus, $\mathbf{c}_{m,j}$, $\theta_{m,j}$, and λ_m are the grid cell's spatial phase offset, orientation offset, and scaling ratio. Grid cell orientations were taken to be ideal values about which the measurements presented in [6] fluctuate, $\theta_{m,j} \in \{-60^\circ, 0^\circ, 60^\circ\}$. Z is a normalizing constant (≈ 2.857399), and f_{\max} is the grid cell's maximum firing rate. In two dimensions, place cells have bivariate Gaussian tuning curves, with mean $\boldsymbol{\xi} \in [0, L] \times [0, L]$, correlation, $\rho \in [-\frac{1}{2}, \frac{1}{2}]$, and covariance $\begin{pmatrix} \sigma_1^2 & \rho\sigma_1\sigma_2 \\ \rho\sigma_1\sigma_2 & \sigma_2^2 \end{pmatrix}$, where σ_1 and σ_2 are chosen from the same range as the standard deviation in the 1D case.

A hybrid codebook: C codewords, of length $N = P + \sum_{m=1}^M J_m$, are generated by quantizing positions on a linear track of length L , and represents the states of the grid and place cells when stimulated with these positions. That is, in 1D, the hybrid code is given by $\mathcal{C} = \{\mathbf{x}(\ell) : \ell \in \{0, \Delta L, 2\Delta L, \dots, (C-1)\Delta L\}\}$, where $\Delta L = L/C$ is the distance between sequential quantized positions. In 2D, \mathcal{C} is constructed by choosing locations, \mathbf{l} , from the vertices of a square lattice imposed on the plane, with unit area equal to $(\Delta L)^2$, and total area equal to L^2 . Code rate, $r = \frac{C}{N}$ (number of represented locations per neuron), measures spatial information resolution, i.e., for a fixed L , a higher code rate, r , is obtained by lowering ΔL .

2.2 De-noising network

Two high capacity associative memory designs are considered to test the hybrid code's resilience to noise. In each case, the memory network is a bipartite graph consisting of N pattern neurons (i.e. grid and place cells) and n_i interneurons. In the unclustered design, all interneurons are connected to a random set of pattern neurons. In the clustered configuration, the interneurons were split into M distinct clusters of n interneurons per cluster, with each cluster connected to a distinct grid module. Each cluster's interneurons were connected randomly to pattern neurons, chosen from a set consisting of every grid cell in the corresponding module, and every place cell.

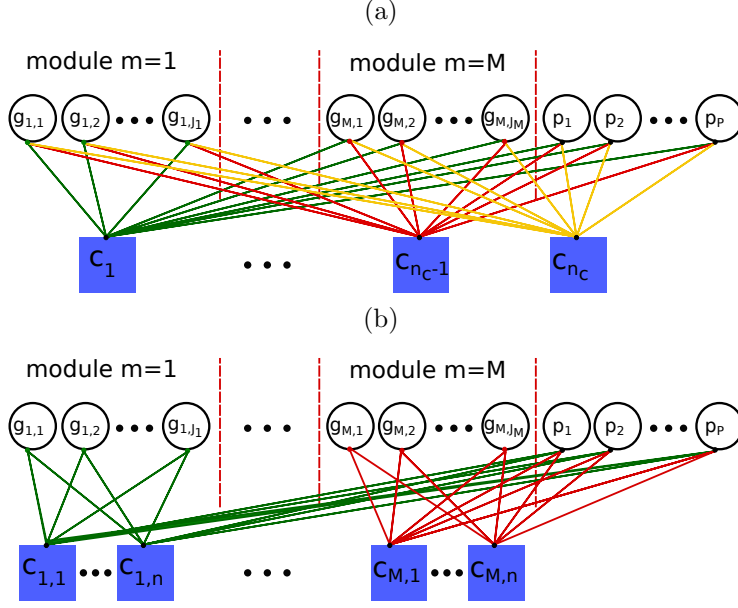


Figure 2: (a) Structure of an un-clustered de-noising network - considered as a baseline for comparison to the neurophysiologically inspired systematic clustering scheme (b) Structure of a systematically clustered de-noising network

We also consider a foil to this systematic clustering scheme: Grid and place cells are randomly assigned to clusters. Figures 2a and 2b depict the general connectivity structure of the un-clustered and clustered designs, respectively. In both the clustered and unclustered configurations, a neurally plausible modified version of Oja’s subspace learning rule was applied to learn the code, i.e. a sparse connectivity matrix is found such that the weights of connections from interneurons to pattern neurons lie orthogonal to the code space (i.e., the space spanned by \mathcal{C}) [16]. This way, interneuron connectivity converges to the parity structure of the code and may be utilized in de-noising operations.

3 Coding theoretic results

We begin our investigation of coding theoretic properties of the hybrid code by defining two measures of redundancy for grid cells: μ_p and μ_o . Define μ_p , be a hybrid code configuration’s spatial phase multiplicity, as the number of grid cells with the same phase in the same module. In [17], it is revealed that there may be a highly non-uniform distribution of phases among grid cells. Replication of phases allows us to investigate coding theoretic repercussions of this phenomenon. We also set $\mu_o = \lfloor \frac{J_1}{3} \rfloor$, the code’s orientation multiplicity (i.e. minimum number of replications of a orientation offset in the first module). These replications are the main sources of grid cell redundancy under consideration. We compare the systematic distributions of grid cell orientation and phase to uniformly random choices for each. Inspired by [18], in order to investigate previously unexplored properties of the grid cell component of the hybrid code, for each of these schemes, we consider two distributions of grid cells to modules: uniform and non-uniform. In the non-uniform

case, $J_m \propto \frac{1}{\lambda_m}$. A scaling ratio of λ defines the scale of module m as $\lambda_m = \lambda_1(\lambda)^{m-1}$. Neural recordings show that the smallest scale is $\lambda_1 \approx 40\text{cm}$ (the value used here) [6].

We construct a codebook matrix, $\underline{\mathbf{C}}$, by placing elements of \mathcal{C} in its rows. We computed normalized rank of the code, $R = \frac{\text{rank}(\underline{\mathbf{C}})}{N}$ as a function of the grid scaling ratio. Normalized rank is an indicator of a code’s density, expressed as the fraction of possible code space occupied by a particular code. The grid cell code is known to be dense [2]. This is especially pronounced when all orientations and phases are chosen randomly (uniformly from $[0, 2\pi]$ and $[0, L] \times [0, L]$ respectively), where for all choices of other parameters, the hybrid code achieves full rank at low rate. When only phases are chosen randomly, but orientations are chosen in accordance with the results in [6], rank is also large at small rates (but not necessarily 1). When orientations are chosen randomly, but phases are uniformly and deterministically distributed, there are hybrid codes with low ranks at plausible rates. When $\mu_p = 1$, a hybrid code with no place cells achieves the largest normalized rank. Further, since place cells communicate redundant information, their inclusion also reduces rank, which is precisely the trend observed in Figure 3. However, this appears to reverse when $\mu_p > 1$, for a sufficiently small number of participating place cells. This occurs because rendering grid cells redundant lowers the rank of the grid-only hybrid code. Consequently, including place cells increases rank, until the information contributed by the place cells reaches its maximum, at which point the inclusion of additional place cells only lowers rank. In contrast to the uniformly allocated grid cells, non-uniformity shifts the rank curve up, though the effect is less pronounced as μ_p increases. In all cases, for a fixed rate, code rank has little dependence on λ . Figure 4 illustrates the influence of μ_o on rank. Increasing μ_o decreases rank, even for less dramatic increases than those shown. This is really because increases in μ_o correspond to decreases in code rate, which lowers rank for most hybrid codes considered. Error bars (measuring SEM) are included due to the stochastic nature of instantiating certain hybrid code parameters (e.g. ξ , which is always chosen uniformly randomly from the set of quantized locations).

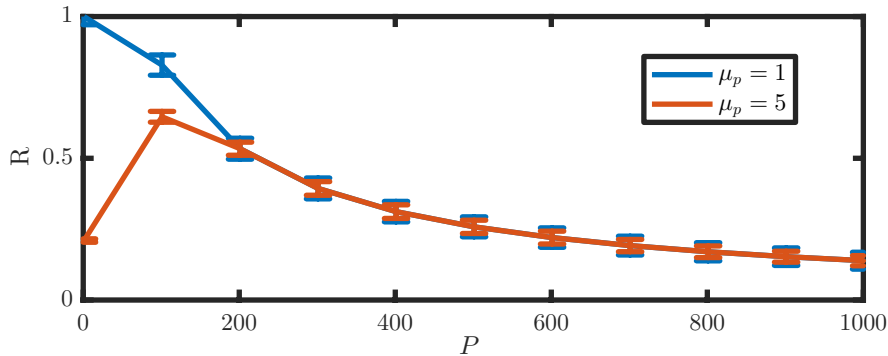


Figure 3: Code rank (R) vs. number of place cells, P , for the hybrid code in 2D, with a uniform allocation of grid cells; here (and in any other plot containing them) error bars show standard error of the mean

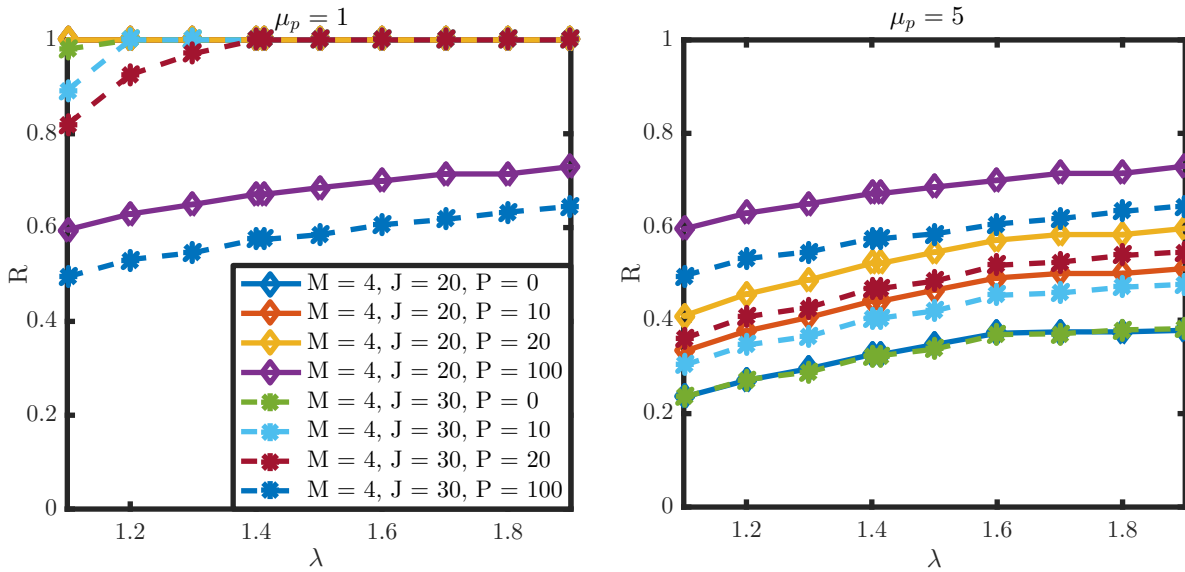


Figure 4: Code rank (R) vs. scaling ratio (λ) for the hybrid code in 2D, a non-uniform allocation of grid cells to modules for $r = 1$, for $\mu_o \in \{6, 10\}$

We also computed rank, R , as a function of code rate, r . When phases are chosen randomly, low rank is difficult to obtain at all but the smallest of code rates tested ($r \in [0, 1]$ and $\mu_p > 1$ may result in low ranks if enough place cells are included). This indicates that biologically reasonable redundancy reduces dimensionality so low ranks are achievable even at high rate. Non-uniformity of the grid cell distribution (to modules) shifts this curve upwards in all cases except that in which phases are chosen randomly, while orientations are chosen deliberately. Later, it will be shown that this low dimensionality is important in constructing sparse and readily de-noisable representations of space. Figure 5 demonstrates that without the redundancy introduced by increasing $\mu_p > 1$, a hybrid code that encodes in 90 neurons more than 90 locations in a $9 m^2$ environment has full rank. However when $\mu_p > 1$, there is a stark drop in the maximum rank achieved. Increasing code rate further after the rank has saturated at one plateau eventually results in a marginal increase in rank. As shown, when $\mu_p > 1$, one may encode orders of magnitude more locations while maintaining low dimensionality, with relatively few cells. This trend is observed in all configurations when appropriate replication of grid phase is ensured. Therefore both dense and sparse hybrid codes may be instantiated by proper choice of population size and redundancy parameters.

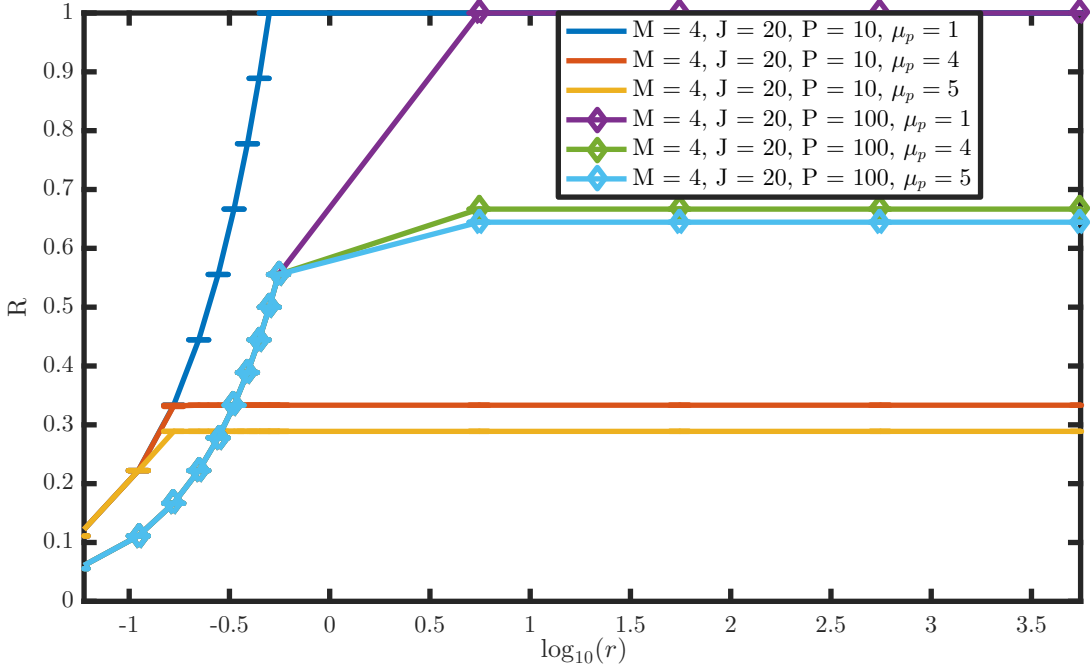


Figure 5: Code rank (R) vs. log of code rate ($\log_{10}(r)$) for the hybrid code in 2D, for $\mu_o = 6$

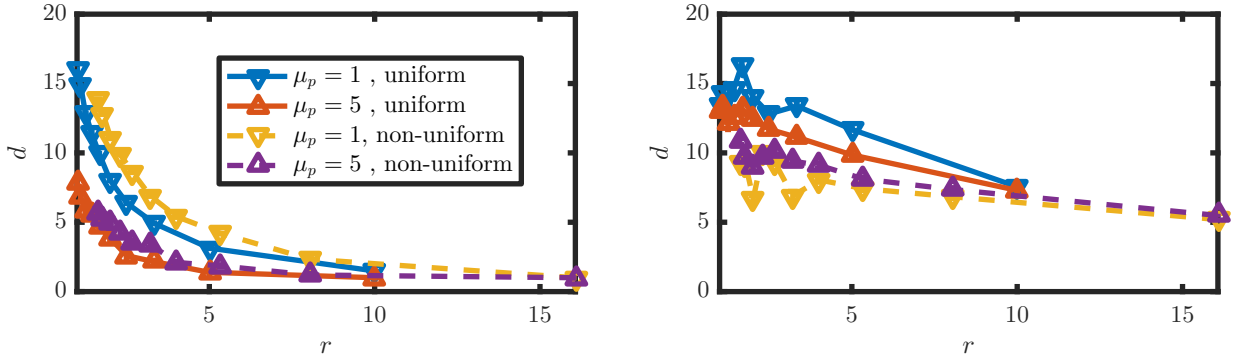


Figure 6: Minimum distance (d) vs r for the hybrid code in 1 and 2 dimensions, with $M = 4$, $J = 20$, and $P = 10$, with deliberately organized grid cell phases and orientations

The code's resilience to neural noise can be assessed by the minimum pairwise (euclidean) distance between codewords, (d). Higher d (i.e., larger distances between codewords) corresponds a more noise tolerant neural representation of space. We computed d as a function of rate, r , for different grid scales (Fig. 6). For any λ , the there is a trade-off between d and r , which highlights the dynamic nature of the code. Since rank tends to increase, with rate, this is also a tradeoff between d and R . When the rate is low (a low resolution of location is targeted), d is larger, so noise tolerance is larger. For a fixed r , a lower rank yields a stronger minimum distance, and lower rates give more desirable tradeoffs between rank and d . For a typical hybrid codebook, for any code rate, d exhibits little dependence on λ . The hybrid code for two-dimensional space performs no worse than the hybrid code for one-dimensional space, and generates a better d for large code

rates in all configurations. Further, in 2D, the code with non-uniformly allocated grid cells has significantly smaller d for a fixed r , while in 1D, this code achieved the largest d with $\mu_p = 1$. Thus, in 2D, for a fixed r (i.e. for codes of the same rate), the code with uniformly allocated grid cells should exhibit measurably better de-noising performance. We confirm this prediction by simulating the de-noising process and collecting statistics presented in Figures 10 through 14. In contrast to a uniform distribution of grid cells to modules, non-uniformity shifts the curve down and to the left (though in 1D, this shift is up and to the right). This is no surprise since non-uniform allocation decreases the total number of grid cells. Increasing μ_p results in marginal decreases in d , though d is less sensitive to increases in phase redundancy than decreases in population size (i.e. codeword length).

For environments of a fixed size, $x_{\max}^2 \text{cm}^2$, and a hybrid code with N neurons, varying code rates implies quantizations of space with varying unit width ($\Delta L = \frac{x_{\max}}{\sqrt{C}}$). Since rate, $r = \frac{C}{N}$, $\Delta L = \frac{x_{\max}}{\sqrt{Nr}}$. Thus the spatial sampling period, ΔL is inversely proportional to \sqrt{r} . In order to ensure we probed reasonable code rates, we estimate the typical perceivable spatial period of a rat by considering its running speed (ranging from .1 to 100 $\frac{\text{cm}}{\text{s}}$), and average ISI of 150ms, which bounds neural sampling periods for space, implying that ΔL should lie somewhere in $[0.15, 15] \text{cm}$. Code rates considered in this work assume $\Delta L < 15 \text{cm}$. To satisfy curiosity, and probe rate dependent phenomena at even greater rates, the smallest ΔL considered is 0.0022cm.

4 Code construction via subspace learning

4.1 Code learning algorithms

Before we can use the de-noising system to correct corrupted codewords, it must learn (i.e. adapt its weights for) the hybrid code. This process is complete when the interneurons may be read to determine if the states of the pattern neurons map to a valid codeword. Formally, this amounts to finding a connectivity matrix, W ($W_{i,j}$ is the synaptic weight between interneuron i and pattern neuron j), whose rows are approximately perpendicular to the code space. A procedure to procure such a matrix is outlined in [16], and improved in [11]. These algorithms begin with a random set of vectors, and for each, seeks a nearby vector orthogonal to \mathcal{C} (i.e. a vector onto which each element of \mathcal{C} has minimal projection). We implement this in Algorithm 1 (a derivation of this algorithm can be found in the appendix). In the clustered design, Algorithm 1 is applied to each cluster's local connectivity matrix. Note that here, all arithmetic on the synaptic weights, $W_{i,j}$ is performed in \mathbb{R} , while arithmetic on states of neurons (i.e. their firing rates), is quantized to the nearest integer in $[0, Q - 1]$. The maximum firing rate, $Q - 1$, is identical for all neurons. With each update, $\mathbf{w} \leftarrow \mathbf{w} - \alpha_t(y(\mathbf{x} - \frac{y\mathbf{w}}{\|\mathbf{w}\|^2}) + \eta\Gamma(\mathbf{w}, \theta))$, where θ is a sparsity threshold, η is a penalty coefficient, $y = \mathbf{x}^T \mathbf{w}$ is the scalar projection of \mathbf{x} onto \mathbf{w} , and α_t is the learning rate at iteration t . Γ is a sparsity enforcing function, approximating the gradient of a penalty function, $g(\mathbf{w}) = \sum_{k=1}^m \tanh(\sigma \mathbf{w}_k^2)$, which, for appropriate choices of σ , penalizes non-sparse solutions early in the learning procedure [11].

Algorithm 1 Neural Learning

Input: set of C patterns, \mathcal{C} , stopping point, ϵ

Output: learned weights matrix, W

```
1: for rows,  $\mathbf{w}$ , of  $W$  do
2:   for  $t \in \{1, \dots, T_{\max}\}$  do
3:      $\alpha_t \leftarrow \max\{\frac{50 \cdot \alpha_0}{50 + \log_{10}(t)}, 0.005\}$ 
4:      $\theta_t \leftarrow \frac{\theta_0}{t}$ 
5:     for  $\mathbf{c} \in \mathcal{C}$  do
6:        $y \leftarrow \mathbf{c} \cdot \mathbf{w}$ 
7:       if  $\|\mathbf{c}\| > \epsilon$  then
8:          $\alpha_t \leftarrow \frac{\alpha_0}{\|\mathbf{c}\|^2}$ 
9:       end if
10:       $\mathbf{w} \leftarrow \text{Dale}(\text{update}(\mathbf{c}, \mathbf{w}, \alpha_t, \theta_t, \eta))$ 
11:    end for
12:    if  $\|\underline{C}\mathbf{w}'\| < \epsilon$  then
13:      break
14:    end if
15:     $t \leftarrow t + 1$ 
16:  end for
17:  for components,  $w_i$  of  $\mathbf{w}$  do
18:    if  $|w_i| \leq \epsilon$  then
19:       $\mathbf{w}_i \leftarrow 0$ 
20:    end if
21:  end for
22: end for
```

As in [11], to speed up learning, we approximate $\Gamma = \nabla g$ with

$$\Gamma(w_t, \theta_t) = \begin{cases} w_t & : |w_t| \leq \theta_t \\ 0 & : \text{otherwise} \end{cases}$$

This update rule is a an improved approximation to Oja's Hebbian learning algorithm [16], with advantages in both biological plausibility and computational complexity. For connections of fixed type (i.e. inhibitory vs excitatory), Oja's rule alone is biologically dubious without the inclusion of many interneurons to manage this change in type. Dale's Principle states that real synaptic connections change type rarely, if ever [19]. In accordance with this principle, our update rule does not allow weights to change sign. This is accomplished after the updated weights are determined: If the sign has changed after applying the update, set the new weight to a value just above (resp. just below) zero if the previous weight was positive (resp. negative). Thus, when learning is complete, these weights will be small in magnitude and are thresholded to zero.

In Algorithm 1, line 11 terminates the learning process if the sum of the projections of the current weight vector on each pattern is no more than ϵ away from zero, that is, if the current

weight vector is approximately orthogonal to the code space. Lines 17-21 perform a thresholding operation that maps to zero any weight sufficiently small in magnitude. This is primarily to suppress numerical errors and promote consistency, as in Line 11, we use ϵ as a small positive constant. Note that since the weights processed on each iteration are independent of those in other iterations, this algorithm can be readily parallelized so that each interneuron learns its weights simultaneously.

4.2 Code learning results

Typical learned connectivity matrices and their associated degree distributions are found in Figures 7 and 8. These demonstrate that for a typical hybrid code, the clustered network has a sparser connectivity, with less variability in its sparsity compared to the un-clustered network. This is because clustering enforces a tighter limit on the number of pattern neurons to which an interneuron may connect. We simulated an ensemble of 4 modules of 20 grid cells each, together with 20 place cells, which produced the following connectivity matrices and associated degree distributions. Interestingly, in both cases, there are place cells (i.e. pattern neurons with index exceeding 80) that are left unconnected to grid modules via interneurons. An illustration of the learned weights matrix corresponding to a randomly clustered de-noising network was omitted, as it is sparser, but otherwise very similar to that of the un-clustered weights image.

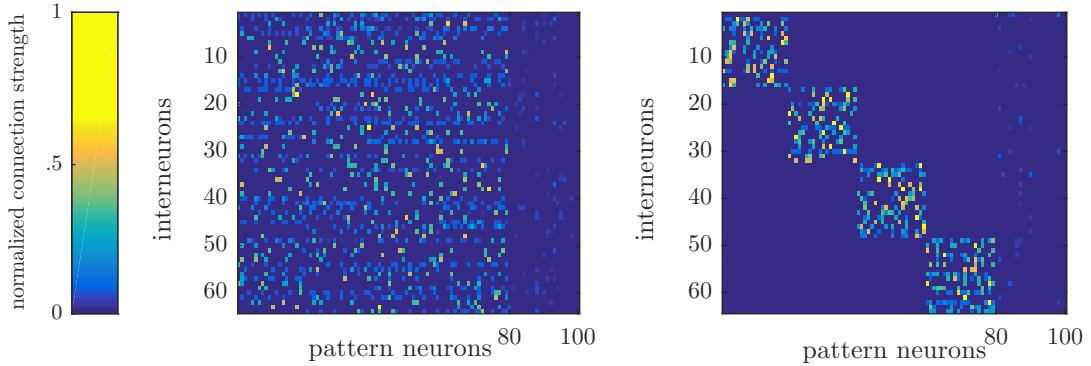


Figure 7: Image of typical weights matrices learned by the de-noising network for a hybrid code with $M = 4$, $J = 20$ and $P = 20$, with modular clustering on the right

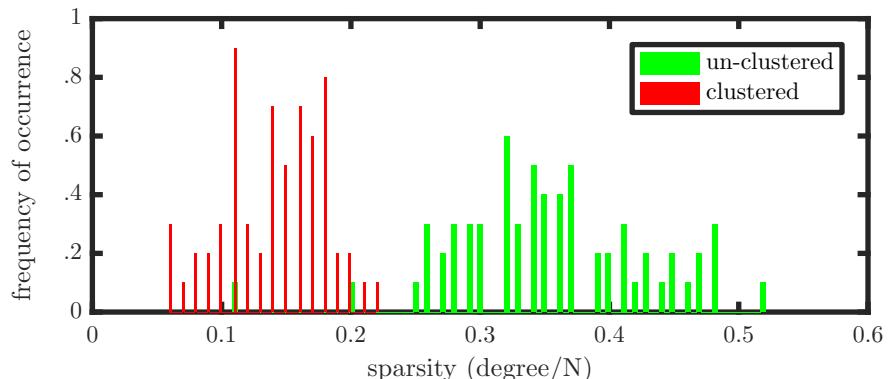


Figure 8: Degree distributions of the connectivity matrices shown in Figure 7

Figure 9 depicts the average connection strength between place cells and grid modules, where the connection strength between place cell p and grid module m is defined as $\frac{1}{n_i}(\sum_{(i,j)} |w_{i,j}w_{i,p}|)$, where i indexes interneurons, and j indexes grid cells in module m . Note here that connectivity does not imply direct synaptic connection, but effective connectivity through interneurons. Results were obtained from configurations with $M = 4$, $J = 20$ and $P = 20$; place cells in legend are ordered by increasing receptive field size; connectivities depicted are averaged over 50 networks. Place cells are ordered by increasing size of receptive field. This trend appears for any $\mu_p > 1$. In the modularly clustered case, average connectivity (between place cells and all grid modules) appears to decrease with increasing place cell size, as compared to a random clustering which produces nearly the same connectivity for each place cell. This phenomenon was not observed when grid phases or grid orientations were chosen randomly. It does not appear in the un-clustered configuration.

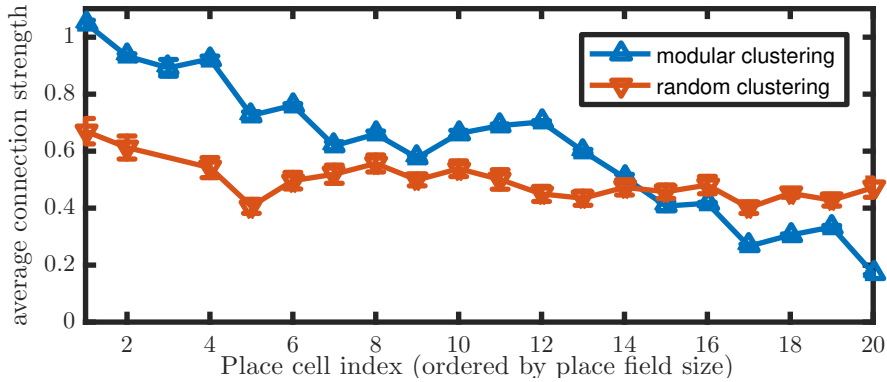


Figure 9: Average connectivities between place cells (x-axis) and grid modules for configurations with $M = 4$, $J = 20$, and $P = 20$; place cell indices are ordered from smallest to largest receptive field size; grid cell phases were uniformly distributed across the environment and grid orientations in agreement with the data presented in [6]; connectivities depicted are averaged over 50 networks

5 De-noising and decoding

5.1 De-noising and decoding algorithms

We implemented a Bit Flipping style neural de-noising process, which we applied to both the clustered and un-clustered de-noising networks. For all configurations (clustered and un-clustered, and for a fixed maximum number of de-noising iterations, the bit flipping algorithm has proven to perform no worse than winner-take-all. Moreover, since it requires only the implementation of additional parallel thresholding operations for each pattern neuron, its implementation is no less biologically feasible. The goal of this algorithm is to recover the correct activity pattern, \mathbf{x} , which has been corrupted by noise, and as such, is currently (and errantly) represented by a noisy version, $\mathbf{x}_n = \mathbf{x} + \mathbf{n}$, where \mathbf{n} is this noise pattern. Since each weight vector is nearly perpendicular to every pattern, for a matrix of weights, W , $\mathbf{x}_n W'$ reveals inconsistencies in \mathbf{x}_n , which the de-noising algorithm seeks to correct in the feedback stage ¹. The clustered de-noising

¹To see this, consider that $\mathbf{x}_n W' = (\mathbf{x} + \mathbf{n})W' = \mathbf{x}W' + \mathbf{n}W' \approx 0 + \mathbf{n}W'$

process begins with Algorithm 3, in which each cluster attempts to detect errant pattern neurons. If no errors are detected, the process is complete. Otherwise, algorithm 2 is invoked for each cluster that detected errant neurons. Note that this de-noising mechanism differs from error correction methods presented in [2] and [12] in that information contributed by place cells only reaches grid cells through interneurons, and place information contributed by grid cells at module i only reaches other modules through interneurons if connectivity (i.e. the hybrid code) allows.

In order to quantify the information content of the population, we estimated the location encoded by the population using a maximum likelihood decoder in 4 different schemes. Joint hybrid decoding utilizes information from all cells. Grid (resp. place) only decoding utilizes information from only grid (resp. place) cells. Grid decoding conditioned on place response performs decoding using only information provided by the grid cells, however, the only candidate locations considered for the estimate are those that are not impossible given the place cell activity.

Algorithm 2 Modular Recall

Input: local weights for this cluster, W , maximum number of iterations, T_{\max} , noisy subpattern, \mathbf{x} , feedback threshold, ϕ

Output: denoised subpattern, \mathbf{d}

```

1:  $\mathbf{d} \leftarrow \mathbf{p}$ 
2: while  $t < T_{\max}$  do
3:    $\mathbf{y} \leftarrow \mathbf{x}W'$ 
4:    $\mathbf{r} \leftarrow \mathbf{y}'W$ 
5:   if  $\|\mathbf{y}\| < \epsilon$  then
6:     break;
7:   end if
8:    $\mathbf{f} \leftarrow \frac{|\mathbf{y}'| \cdot |W|}{\sum_{i=1}^m |W|}$ 
9:   for each pattern neuron,  $j$  do
10:    if  $\mathbf{f}_j \geq \phi$  then  $\mathbf{f}_j = \text{sign}(\mathbf{x}_j)$ 
11:    else  $\mathbf{f}_j = 0$ 
12:    end if
13:  end for
14:   $\mathbf{d} \leftarrow \mathbf{d} + \mathbf{f}$ 
15: end while
```

Algorithm 3 Sequential de-noising

Input: local weights, W_i , for each cluster, $i \in \{1, \dots, M\}$, noisy pattern, \mathbf{x}_n , stopping threshold, ϵ

Output: denoised pattern, \mathbf{x}_d

```
1:  $\mathbf{x}_d \leftarrow \mathbf{x}_n$ 
2: while  $t < T_{\max}$  and a cluster has an unsatisfied constraint do
3:   for each cluster,  $i \in \{1, \dots, M\}$  do
4:      $\mathbf{x} \leftarrow$  subpattern corresponding to cluster  $i$ 
5:      $\mathbf{d} \leftarrow \text{Modular\_Recall}(\mathbf{x}, W_i)$ 
6:     if  $|\mathbf{d}W_i| \leq \epsilon$  then
7:        $\mathbf{x}_d(\text{cluster } i\text{'s subpattern indices}) \leftarrow \mathbf{d}$ 
8:     end if
9:   end for
10:   $t \leftarrow t + 1$ 
11: end while
```

5.2 De-noising and Decoding Results

To measure the denoising performance of this system, we first perturb the states (i.e. firing rates) of the grid and place cells by incrementing or decrementing randomly and clipping to the boundaries of $[0, Q - 1]$. A pattern error occurs if after de-noising, any entry of the de-noised pattern differs from the corresponding component of the original pattern. A symbol error occurs each time any symbol of the de-noised pattern differs from the corresponding symbol of the correct pattern. For identical populations of grid and place cells ($M = 4$, $J = 20$, and $P = 10$), in pattern error rate, the clustered network dramatically outperforms the un-clustered (when the grid cells have sufficient redundancy), and the modular clustering scheme always outperforms the random clustering scheme. Figure 10 depicts pattern error rate (P_{pe}) for a clustered hybrid code, with varying phase multiplicity and biologically consistent orientation multiplicity. All other configurations (that is, those configurations that did not employ clustering in de-noising, or had randomly selected phases or randomly selected orientations) had 100 percent pattern error rate even for a small number of initial errors. This shows that for a small number of initial errors, the full pattern of population activity corresponding to the correct location may be recovered, but that for many noise-induced errors, this is rarely possible. That only the modularly clustered de-noising network is able to achieve low P_{pe} (and only when μ_p is large enough) shows that the biological organization of grid cells into discrete modules, is important for high quality self location in the presence of noise. Further, clustering is the only way to achieve such a small P_{pe} , since no non-clustered de-noising network consistently reduces P_{pe} below 0.99. It is no surprise that for a small number of errors, the modularly clustered de-noising mechanism achieves a better P_{pe} when de-noising hybrid codes with uniform allocations of grid cells to modules (as compared to non-uniform allocations of grid cells to modules), as Figure 6 demonstrates that such codes tend to have a larger minimum distance at any rate probed. This result also demonstrates that whether or not grid cells are distributed uniformly to modules has a smaller impact on P_{pe} than μ_p .

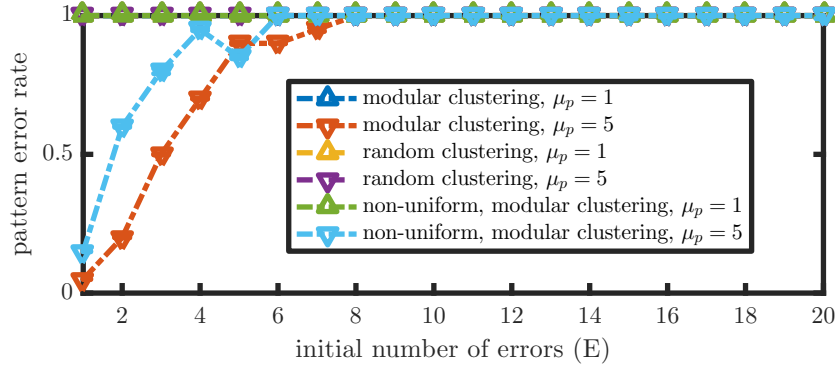


Figure 10: Pattern error rate vs. initial number of errors for a clustered hybrid code with $M = 4$, $J = 20$, $P = 10$, with deliberately chosen spatial phases and orientations; all other pattern error rates tested (i.e. those with random redundancy parameters or those with a non-clustering denoising network) have $P_{pe} = 1$ for any initial number of errors

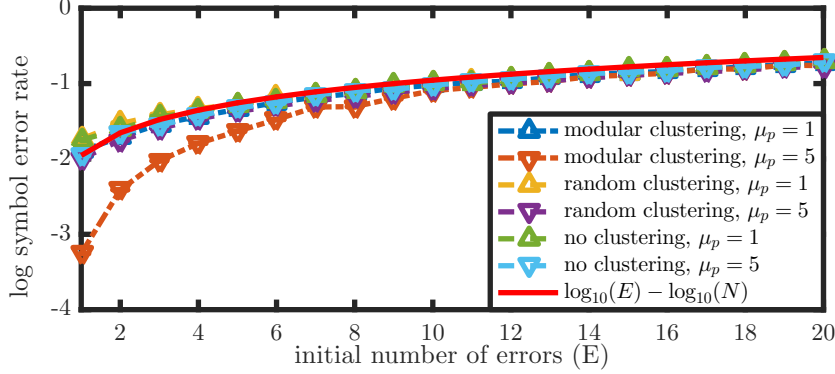


Figure 11: Symbol error rate vs. initial number of errors for clustered and non-clustered hybrid codes; here, each code utilizes a uniform distribution of grid cells to modules, and deliberately chosen spatial phases and orientations

Figure 11 shows symbol error rates of hybrid codes for several configurations with deliberately chosen grid cell phases and orientations. This demonstrates that generally, clustered de-noising networks do not offer improved symbol error rate, P_{se} , compared to their un-clustered counterparts. However, for a small initial number of errors, when the grid cells exhibit sufficient redundancy in their phases, a randomly clustered de-noising network is only outperformed by a modularly clustered network. Figure 12 shows P_{se} for a hybrid code with deliberately chosen phases and orientations, de-noised by a modularly clustered network. Consistent with the observations on pattern error rate, hybrid codes with grid cells uniformly allocated to modules achieve better P_{se} . This may result directly from the fact that d is larger for such codes. On the other hand, it is possible that the smaller population sizes resulting from a non-uniform allocation (thus allowing fewer opportunities for grid cell redundancy) are behind both the improvement in denoising performance and the larger minimum distance. Plotted in both Figures 11 and 12 is a red, solid curve, $\log_{10}(\frac{\text{initial number of errors}}{N})$. This curve is a threshold between regions of desirable and unacceptable

P_{se} (i.e. $\log_{10}(P_{se})$ for a network that performs no de-noising). To see this, consider a de-noising network that does not change the initial number of errors, E . For this network, $P_{se} = \frac{E}{N}$, so $\log_{10}(P_{se}) = \log_{10}(E) - \log_{10}(N)$. Surprisingly, figure 11 shows that for a small initial number of errors, configurations with $\mu_p = 1$ have $\log_{10}(P_{se})$ above this threshold, that is, they increase the number of symbol errors! Figure 12 shows that this observation is independent of uniformity of the distribution of grid cells to modules.

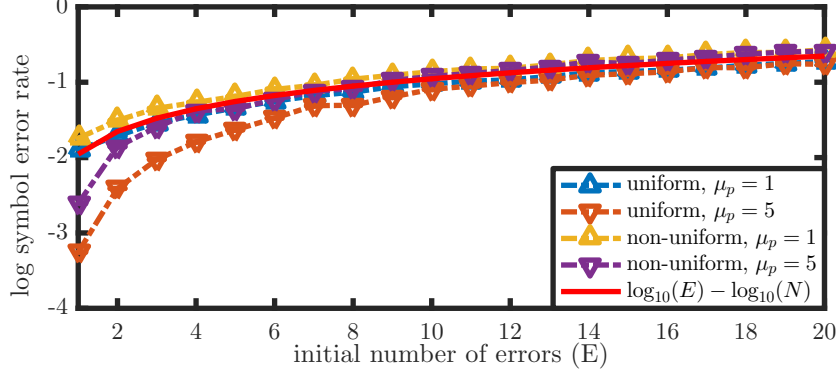


Figure 12: Symbol error rate vs. initial number of errors for uniform and non-uniform clustered hybrid codes; here, each de-noising network employs the modular clustering scheme

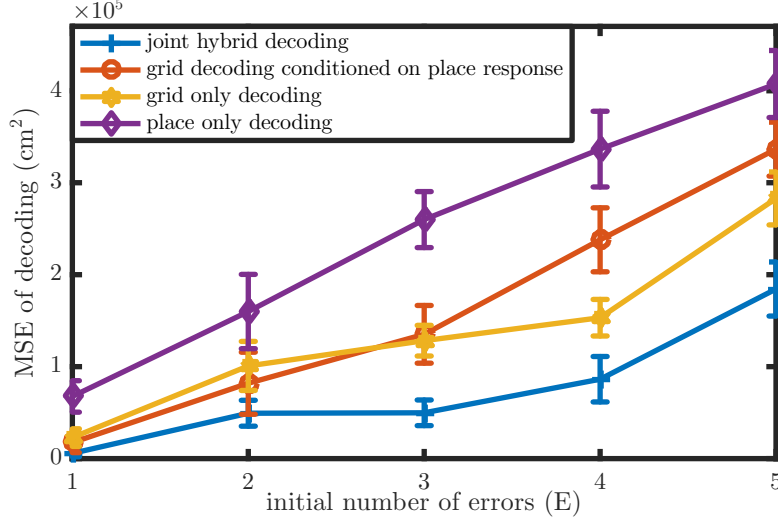


Figure 13: MSE of decoding after de-noising for a hybrid code with $M = 4$, $J = 20$, $P = 10$, and $\mu_p = 5$, for position in 2D, and deliberately chosen grid cell parameters

Figure 13 shows MSE of different decoding processes after de-noising for a Hybrid code with $M = 4$, $J = 20$, $P = 10$, and $\mu_p = 5$, for position in 2D, and deliberately chosen grid cell parameters. This plot demonstrates that an ideal observer decoder which considers information from all cells outperforms all others for any initial number of errors. This disparity may, in part, be accounted for by the difference between the number of grid cells and the number of place cells. Figure 14 shows MSE of joint hybrid decoding after de-noising for a hybrid code with $\mu_p = 5$,

with position in 2D, for the configuration that achieved the best error correction performance in both P_{pe} and P_{se} . This plot demonstrates that the code with grid cells distributed to modules uniformly, with a modularly clustered de-noising network achieves the best decoding performance, outperforming its non-uniformly distributed analogue. Since in 2D the code with a non-uniform allocation of grid cells to modules had a smaller minimum distance (compared to the same code with a uniform allocation of grid cells to modules), this result confirms our hypothesis that codes with larger d may be de-noised more effectively. Further, this demonstrates (in a natural metric of the stimulus space) that in the most redundant hybrid code considered, a modularly clustered de-noising network is far superior to a randomly clustered or un-clustered one. These results are unsurprising given the P_{pe} and P_{se} data presented earlier.

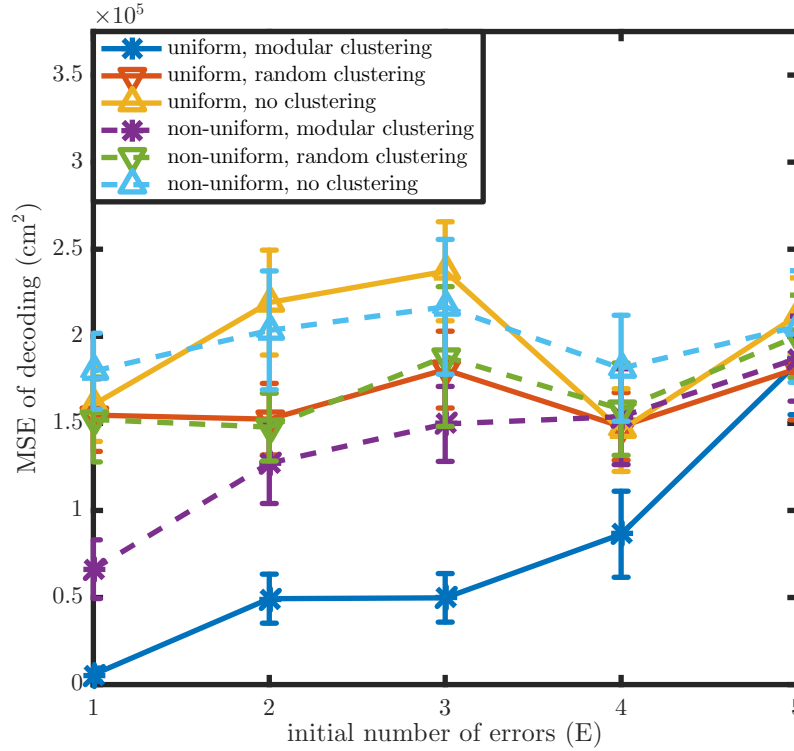


Figure 14: MSE of decoding after neural de-noising (cm^2) vs initial number of errors for a hybrid code with $\mu_p = 5$ and $\mu_o = 6$.

6 Discussion

We demonstrated that both dense and sparse hybrid codes may be constructed by proper choice of grid and place cell parameters. We also showed that in the presence of neural noise, the activity of only some of these configurations may be consistently de-noised. It is somewhat surprising that choosing $\mu_p > 1$ produces a more noise resilient code (as shown in the de-noising performance results) as the 2D hybrid codes with uniformly allocated grid cells and largest d are those with unique spatial phases (i.e. $\mu_p = 1$) (Figure 6). Further, this observation demonstrates that the hybrid code for space may trade off efficiency of encoding, R , for improvements in de-noising

performance by distributing grid cells to modules non-uniformly [18]. Hybrid codes of widely varying R , d , and r may be instantiated by choosing appropriate parameters for the populations of grid and place cells, a fact that showcases the code’s adaptability. This means that the grid and place cells may be chosen for participation in neural computations, whose performance relies on assumptions other than those presented here, which insist on a low dimensional code space, and a sparse connectivity matrix.

We demonstrate that the chosen de-noising network architecture performs quite well for hybrid codes that fit its assumptions regarding rank, and poorly for those that do not. Additionally, we assessed average connectivity between place cells of varying receptive field sizes and modules of grid cells by analyzing the learned connectivity matrix. This analysis demonstrates that our model place cells of smaller receptive field size are more strongly connected to grid modules, and that they are most strongly connected to grid modules of the smallest scale. Such a result presents a physiologically testable hypothesis. While difficult, two photon microscopy has been successfully employed to accurately image the microscopic structure of nervous tissue [20]. One way to estimate connection strength between real neurons is to count the number of boutons expressed on the pre-synaptic neurons, assuming that weight should be proportional to this number, though there are certainly easier ways to estimate connection strength [21]. Thus, if groups of place cells connected via interneurons to several distinct grid modules may be identified, this theoretical prediction can be confirmed or refuted. Another interesting experiment is made possible by recent advances in optogenetics, which enable single cell resolution of network activity for a population of inoculated cells (e.g. a collection of grid cells, as in [22]). While technically challenging due to the physical separation of each population in the brain, it should be possible to image simultaneous activity of grid and place cells at high temporal precision [23]. From these measurements, for a set of quantized locations, simultaneous firing rates may be estimated [24]. Then, the rank, rate, and minimum distance of this empirical codebook may be computed to offer insight about limits of noise tolerance of real spatial navigation circuitry. Of particular interest is discovering the extent to which neural noise transiently varies such attributes for grid and place cells in real brains, and how these coding theoretic properties adapt (if at all) to changes in speed, context, and other variables.

In Figures 10, 12, 13, and 14, we demonstrate the differences in performance of each network structure, and of the various decoding algorithms. The universal improvements from place only decoding to joint hybrid decoding show that highly accurate position estimation can be significantly more difficult without both populations of cells. The discrepancy between ‘grid only decoding’ and ‘grid decoding conditioned on place response’ shows that even utilizing place cell information indirectly (by eliminating places deemed impossible given the state of the place cell population) yields a sizable improvement in decoding accuracy when there are many place cells, or when place cells are less noisy than grid cells. That the modular clustering network universally outperforms the corresponding randomly clustered network implies that the physiological organization of grid cells by their scale may provide a computational advantage in de-noising and decoding. This may be because the un-clustered network is essentially a randomly clustered network that does not

take advantage of synergistic cluster computing. In any cluster, both grid cells and place cells are able to correct each others' errant activity. However, under modular clustering, in order for a grid cell in module i to correct the activity of a grid cell in a different module j , the activity of each neuron in module i must be correct so that the activity of place cells (connected to both modules i and j) will contradict and correct the erroneous activity. It should be noted here that the de-noising interneurons are a hypothetical construct and need not reside in the hippocampus, or MEC. Furthermore, this work is not intended to convince readers of the necessity or existence of these cells, only to demonstrate tangible coding theoretic advantages to their implementation alongside this neural code for position.

Further development on neural codes for space include studying coding theoretic properties of more complete navigational codes including head direction cells, boundary vector cells, and time cells [25–27]. Even with these classes of neuron, the hybrid code might be unable to encode and de-noise path information, unless there is a higher level structure that provides the encoded activity in the correct sequence. One strong candidate solution for this is to include so called hippocampal time cells. Just as place cells code for distinct locations on paths through space, time cells encode ordered moments in a temporally ordered sequence of events, precisely the information, which, when coupled with location, allows for the encoding of paths [28].

References

- [1] A. D. Ekstrom, M. J. Kahana, J. B. Caplan, T. A. Fields, E. A. Isham, E. L. Newman, and I. Fried, “Cellular networks underlying human spatial navigation,” *Nature*, vol. 425, no. 6954, pp. 184–188, 2003.
- [2] I. R. Fiete, Y. Burak, and T. Brookings, “What grid cells convey about rat location,” *The Journal of Neuroscience*, vol. 28, no. 27, pp. 6858–6871, 2008.
- [3] M. Fyhn, T. Hafting, M. P. Witter, E. I. Moser, and M.-B. Moser, “Grid cells in mice,” *Hippocampus*, vol. 18, no. 12, pp. 1230–1238, 2008.
- [4] M. M. Yartsev, M. P. Witter, and N. Ulanovsky, “Grid cells without theta oscillations in the entorhinal cortex of bats,” *Nature*, vol. 479, no. 7371, pp. 103–107, 2011.
- [5] B. A. Strange, M. P. Witter, E. S. Lein, and E. I. Moser, “Functional organization of the hippocampal longitudinal axis,” *Nat Rev Neurosci*, vol. 15, no. 10, pp. 655–669, Oct. 2014. [Online]. Available: <http://dx.doi.org/10.1038/nrn3785>
- [6] H. Stensola, T. Stensola, T. Solstad, K. Frøland, M.-B. Moser, and E. I. Moser, “The entorhinal grid map is discretized,” *Nature*, vol. 492, no. 7427, pp. 72–78, 2012.
- [7] T. Bonnevie, B. Dunn, M. Fyhn, T. Hafting, D. Derdikman, J. L. Kubie, Y. Roudi, E. I. Moser, and M.-B. Moser, “Grid cells require excitatory drive from the hippocampus,” *Nature neuroscience*, vol. 16, no. 3, pp. 309–317, 2013.

- [8] L. Muessig, J. Hauser, T. J. Wills, and F. Cacucci, “A developmental switch in place cell accuracy coincides with grid cell maturation,” *Neuron*, vol. 86, no. 5, pp. 1167–1173, 2015.
- [9] J. J. Hopfield, “Neural networks and physical systems with emergent collective computational abilities,” *Proceedings of the national academy of sciences*, vol. 79, no. 8, pp. 2554–2558, 1982.
- [10] R. J. McEliece, E. C. Posner, E. R. Rodemich, and S. S. Venkatesh, “The capacity of the hopfield associative memory,” *Information Theory, IEEE Transactions on*, vol. 33, no. 4, pp. 461–482, 1987.
- [11] A. H. Salavati, K. R. Kumar, and A. Shokrollahi, “Nonbinary associative memory with exponential pattern retrieval capacity and iterative learning,” *Neural Networks and Learning Systems, IEEE Transactions on*, vol. 25, no. 3, pp. 557–570, 2014.
- [12] M. Stemmler, A. Mathis, and A. V. Herz, “Connecting multiple spatial scales to decode the population activity of grid cells,” *Science Advances*, vol. 1, no. 11, p. e1500816, 2015.
- [13] A. Karbasi, A. H. Salavati, A. Shokrollahi, and L. R. Varshney, “Noise facilitation in associative memories of exponential capacity,” *Neural computation*, 2014.
- [14] A. Karbasi, A. H. Salavati, and A. Shokrollahi, “Iterative learning and denoising in convolutional neural associative memories,” in *Proceedings of The 30th International Conference on Machine Learning*, 2013, pp. 445–453.
- [15] C. Curto, V. Itskov, K. Morrison, Z. Roth, and J. L. Walker, “Combinatorial neural codes from a mathematical coding theory perspective,” 2012.
- [16] E. Oja and T. Kohonen, “The subspace learning algorithm as a formalism for pattern recognition and neural networks,” in *Neural Networks, 1988., IEEE International Conference on*. IEEE, 1988, pp. 277–284.
- [17] D. Wennberg, “The distribution of spatial phases of grid cells,” 2015.
- [18] N. W. Mosheiff, H. Agmon, A. Moriel, and Y. Burak, “An efficient coding theory for a dynamic trajectory predicts non-uniform allocation of grid cells to modules in the entorhinal cortex,” *arXiv preprint arXiv:1601.02948*, 2016.
- [19] J. Eccles, “From electrical to chemical transmission in the central nervous system,” *Notes and records of the Royal Society of London*, vol. 30, no. 2, pp. 219–230, 1976.
- [20] K. Svoboda and R. Yasuda, “Principles of two-photon excitation microscopy and its applications to neuroscience,” *Neuron*, vol. 50, no. 6, pp. 823–839, 2006.
- [21] G.-q. Bi and M.-m. Poo, “Synaptic modifications in cultured hippocampal neurons: Dependence on spike timing, synaptic strength, and postsynaptic cell type,” *Journal of Neuroscience*, vol. 18, no. 24, pp. 10 464–10 472, 1998. [Online]. Available: <http://jneurosci.org/content/18/24/10464>

- [22] C. Sun, T. Kitamura, J. Yamamoto, J. Martin, M. Pignatelli, L. J. Kitch, M. J. Schnitzer, and S. Tonegawa, “Distinct speed dependence of entorhinal island and ocean cells, including respective grid cells,” *Proceedings of the National Academy of Sciences*, vol. 112, no. 30, pp. 9466–9471, 2015. [Online]. Available: <http://www.pnas.org/content/112/30/9466.abstract>
- [23] B. F. Grewe, D. Langer, H. Kasper, B. M. Kampa, and F. Helmchen, “High-speed in vivo calcium imaging reveals neuronal network activity with near-millisecond precision,” *Nature methods*, vol. 7, no. 5, pp. 399–405, 2010.
- [24] L. Theis, P. Berens, E. Froudarakis, J. Reimer, M. R. Rosón, T. Baden, T. Euler, A. S. Tolias, and M. Bethge, “Benchmarking spike rate inference in population calcium imaging,” *Neuron*, vol. 90, no. 3, pp. 471–482, 2016.
- [25] C. Lever, S. Burton, A. Jeewajee, J. O’Keefe, and N. Burgess, “Boundary vector cells in the subiculum of the hippocampal formation,” *The journal of neuroscience*, vol. 29, no. 31, pp. 9771–9777, 2009.
- [26] D. M. Salz, Z. Tiganj, S. Khasnabish, A. Kohley, D. Sheehan, M. W. Howard, and H. Eichenbaum, “Time cells in hippocampal area ca3,” *Journal of Neuroscience*, vol. 36, no. 28, pp. 7476–7484, 2016.
- [27] J. S. Taube, R. U. Muller, and J. B. Ranck, “Head-direction cells recorded from the post-subiculum in freely moving rats. i. description and quantitative analysis,” *The Journal of neuroscience*, vol. 10, no. 2, pp. 420–435, 1990.
- [28] C. J. MacDonald, K. Q. Lepage, U. T. Eden, and H. Eichenbaum, “Hippocampal ”time cells” bridge the gap in memory for discontinuous events,” *Neuron*, vol. 71, no. 4, pp. 737–749, 2011.
- [29] E. Oja and J. Karhunen, “On stochastic approximation of the eigenvectors and eigenvalues of the expectation of a random matrix,” *Journal of mathematical analysis and applications*, vol. 106, no. 1, pp. 69–84, 1985.
- [30] L. Xu, A. Krzyzak, and E. Oja, “Neural nets for dual subspace pattern recognition method,” *International Journal of Neural Systems*, vol. 2, no. 03, pp. 169–184, 1991.

7 Appendix

7.1 Subspace learning

In [29], the authors propose an algorithm that is capable of computing a basis for the null space of a random matrix, A , which is assumed to be the expected value of sample matrices, A_t . The update rule for the matrix whose columns are the resulting basis vectors is

$$\tilde{W}_t = W_{t-1} + A_{t-1}W_{t-1}\alpha_{t-1} \quad (3)$$

$$W_t = \tilde{W}_t R_t^{-1}, \quad (4)$$

where α_t is a diagonal (and compatible) matrix of gain factors. As in [29], equations 3 and 4 may be re-written as operations on column vectors, \mathbf{w}_t .

$$\tilde{\mathbf{w}}_t = \mathbf{w}_{t-1} + \alpha_{t-1} A_{t-1} \mathbf{w}_{t-1} \quad (5)$$

$$\mathbf{w}_t = \frac{\tilde{\mathbf{w}}_t}{\|\tilde{\mathbf{w}}_t\|}, \quad (6)$$

in which α_t is the gain factor corresponding to the current column. This number may be equivalently understood as a learning rate. Indeed in [30], the authors show that for appropriate choices of A_t , the update rule is a form of anti-Hebbian learning. In [29] the authors prove convergence of this algorithm to the eigenvectors of A corresponding to the largest eigenvalues. Further, when A_t is replaced by $-A_t$, \mathbf{w}_t converges to the eigenvectors of A corresponding to the smallest eigenvalues. In [29], it is demonstrated that by combining equations 5 and 6, expanding as a power series in α_t , and ignoring second (and higher) order terms, we arrive at

$$\mathbf{w}_t = \mathbf{w}_{t-1} + \alpha_{t-1} (A_{t-1} \mathbf{w}_{t-1} - \frac{\mathbf{w}_{t-1}^T A_{t-1} \mathbf{w}_{t-1}}{\mathbf{w}_{t-1}^T \mathbf{w}_{t-1}} \mathbf{w}_{t-1}). \quad (7)$$

The authors of [11] choose $A_t = (\mathbf{x}_t^T \mathbf{x}_t) P_{\mathbf{x}_t} = \mathbf{x}_t \mathbf{x}_t^T$, the product of projections onto the space spanned by \mathbf{x}_t , and define $y_t = \mathbf{x}_t^T \mathbf{w}_t = \mathbf{w}_t^T \mathbf{x}_t$. In [29], it is mentioned that this update rule finds eigenvectors corresponding to the largest eigenvalue of A_t , or those corresponding to the smallest eigenvalues of $-A_t$, when this matrix is used instead. Since A_t is a projection matrix, it has rank 1. Thus it has one eigenvector with non-zero eigenvalue, \mathbf{x}_t , and $\dim(\mathbf{x}) - 1$ eigenvectors with eigenvalue 0. Each of these eigenvectors, \mathbf{v} , is guaranteed to be perpendicular to \mathbf{x} because $A_t \mathbf{v} = 0 \mathbf{v} = \mathbf{0}$, that is, the \mathbf{v} 's projection onto \mathbf{x} has magnitude 0. By choosing $\mathbf{x}_t \in \mathcal{C}$, with the aforementioned choice for A_t , this algorithm should compute vectors approximately perpendicular to the code space.

Now, we may rewrite equation 7 as

$$\begin{aligned} \mathbf{w}_t &= \mathbf{w}_{t-1} - \alpha_{t-1} \mathbf{x}_{t-1} \mathbf{x}_{t-1}^T \mathbf{w}_{t-1} + \alpha_{t-1} \frac{\mathbf{w}_{t-1}^T \mathbf{x}_{t-1} \mathbf{x}_{t-1}^T \mathbf{w}_{t-1}}{\|\mathbf{w}_{t-1}\|^2} \mathbf{w}_{t-1} \\ &= \mathbf{w}_{t-1} - \alpha_{t-1} y_{t-1} \mathbf{x}_{t-1} + \alpha_{t-1} \frac{y_{t-1}^2}{\|\mathbf{w}_{t-1}\|^2} \mathbf{w}_{t-1}. \end{aligned} \quad (8)$$

To obtain a sparse basis for $\text{null}(\underline{\mathcal{C}})$, one may add to equation 8 a regularizing term that penalizes non-sparse solutions. In particular, using $\eta \Gamma(\mathbf{w}_{t-1}, \theta_{t-1})$, as considered in [11], to arrive at

$$\mathbf{w}_t = \mathbf{w}_{t-1} - \alpha_{t-1} (y_{t-1} (\mathbf{x}_{t-1} - \frac{y_{t-1} \mathbf{w}_{t-1}}{\|\mathbf{w}_{t-1}\|^2})) - \alpha_{t-1} \eta \Gamma(\mathbf{w}_{t-1}, \theta_{t-1}). \quad (9)$$

7.2 Choices of parameters

In learning, normalized weights are initialized randomly with degree $\lceil 4 \log_e(n) \rceil$, where n is the length of the weight vector. We used, $\theta_0 = 0.031$, $\epsilon = C10^{-3}$, $\eta = 0.075$, and $\alpha_0 = 0.95$. In de-noising, we set $\phi = 0.95$.